Mon. Not. R. astr. Soc. (1983) **203**, *Short Communication*, 19P–23P

Intrinsic principal axes twists in *N*-body models of elliptical galaxies

Ortwin E. Gerhard *Department of Theoretical Physics, 1 Keble Road, Oxford OX1 3NP*

Received 1983 January 20; in original form 1982 December 13

Summary. We have found intrinsic principal axes twists in two *N*-body models of elliptical galaxies. In one case, this configuration is connected with differential figure rotation and disappears through secular evolution. The second model hardly rotates and the twists persist for $\geqslant 15$ crossing times.

1 Introduction

It is now well known that velocity anisotropy plays an important role in determining the shapes of elliptical galaxies. Thus one may argue that these will, in general, have triaxial figures (Binney 1978b). However, it has until now been generally assumed that the isodensity surfaces of these galaxies have common principal axes. This assumption is consistent with observations of a number of ellipticals with isophote twists and radially varying ellipticities (Carter 1978; King 1978; Bertola & Galetta 1979; di Tullio 1979; Williams & Schwarzschild 1979; Leach 1981). In this paper we argue that this interpretation of the observations may, however, not describe the general case, by presenting two model stellar systems which have intrinsic principal axes twists over astronomically interesting time-scales.

As in a previous paper (Gerhard 1983, Paper II) we use remnants of merging simulations as our models. These are dynamically akin to elliptical galaxies for a range of initial conditions without much dependence on the shapes of the progenitors (White 1978; Gerhard 1981, Paper I). The present *N*-body models have enough resolution ($N = 1000$ and $N = 1500$) to detect major axes misalignments as a function of radius by the simple method described in Paper II.

2 Method and notation

The principal axes **a**, **b**, **c** ($a > b > c$) are found by diagonalizing a unit vector–direction tensor (see Paper II). The program then finds the mean coordinate magnitudes along these axes. These are converted to ellipticities ϵ_b, ϵ_c ($\epsilon_i = 1 - i/a$) by a calibration with Monte Carlo simulations. Typical ellipticity errors found from these simulations are ≈ 0.1, with direction errors depending on ellipticity.

Velocity dispersions along the directions of the principal axes, σ_a, σ_b, σ_c are obtained from sets of particles centred about given points in a suitable superposition of several snap-

shots of the system. We also use the central velocity dispersion $\sigma_0 = \sqrt{\Sigma \sigma_i^2\,(\mathbf{0})}$. The rotational properties of a model are specified by the usual dimensionless spin-parameter $\lambda = G^{-1}|\mathbf{L}||E|^{1/2}M^{-5/2}$ or the ratio v_{max}/σ_0, where E and M are the total energy and mass of the system and v_{max} is the maximum of the rotation velocity $v_r(R)$ measured in cylinders parallel to the angular momentum vector $\mathbf{L}$. The relation between velocity anisotropy, rotation and flattening is given by the tensor virial equations (Binney 1978a). These are strictly true only globally but may be approximately applied locally for dynamically relatively isolated parts of the system.

3 A slowly evolving model with differential figure rotation

This model (hereafter: model ME) was formed through the merger of the model described in Paper II (hereafter: model MA) with another disc–halo galaxy (see Paper I), except that both progenitors did not contain massive core particles. The initial orbit was bound and the

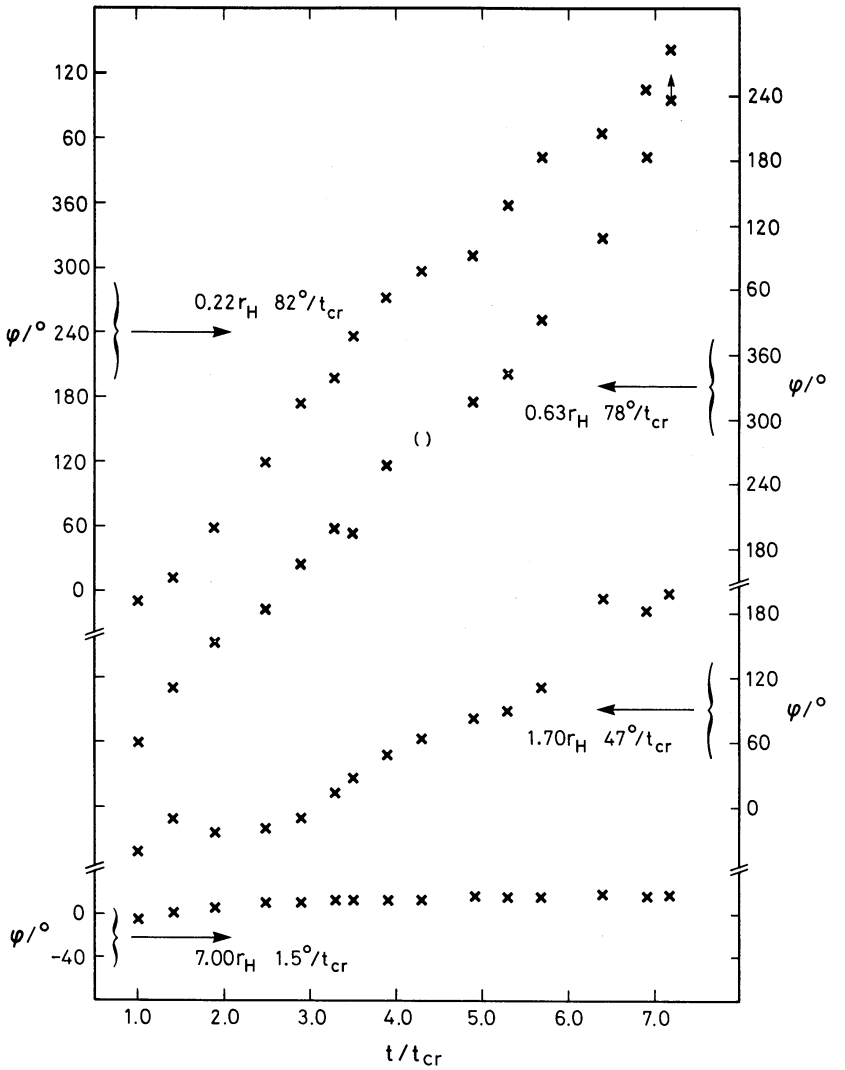

Figure 1. Differential figure rotation in model ME. The angle ϕ between the major axis of all particles in each of four spherical shells and a fixed reference axis in the rotation (major) plane of the 'galaxy' is shown as a function of time. The median radius in units of the half-mass radius of the system and the mean major axis rotation rate per crossing time estimated from the respective curve are also given for each shell.

dominant orbital angular momentum was essentially aligned with the spin vectors of the progenitors. Thus, this is a high angular momentum model ($\lambda = 0.13$, $v_{max}/\sigma_0 = 0.46$) with its minor axis direction close to L and perpendicular to the orbital plane. (These and all subsequent data refer to the entire system, for statistical reasons; the differences between disc and halo particles as defined in Paper I are not very substantial.)

Model ME is triaxial at all radii. Its overall ellipticity in the minor axis direction is $\epsilon_c \approx 0.5$; in the centre we find $\epsilon_c \approx 0.6$. This is mainly a result of velocity anisotropy, in spite of the high angular momentum. In the centre, velocity dispersions and rotation velocity give $s \equiv 2\sigma_c^2/(v_r^2 + 2\sigma_a^2) = 0.51$, corresponding to $\epsilon_c \approx 0.5$ by the tensor virial theorem. In the outer parts, one finds $s = 0.59$, $\epsilon_c = 0.45$. Both predicted values of ϵ_c are slightly smaller than the measured values. Note that anisotropy alone would almost cause a flattening of $\epsilon_c \approx 0.5$ in the centre, but rotation alone only $\epsilon_c \approx 0.2$. The second ellipticity of this model is $\epsilon_b \approx 0.2$, with little radial change, although the direction of the major axis changes radially by substantial angles (see below). At the same time, the velocity dispersions in the major plane are almost isotropic, so that the triaxiality observed is a consequence of the figure rotation described next.

Fig. 1 shows the evolution of the angle between a reference axis in the orbital plane and the major axis defined by the particles in each of four spherical shells, during the first seven crossing times (t_{cr}) after equilibrium was reached. From this diagram, it is clear that figure rotation is rapid in the inner parts and almost absent in the outermost shell. For each shell, the median radius in units of the system half-mass radius r_H and the mean rotation rate estimated from the curves are given on the figure. Table 1 compares the rotation velocities expected from these figure rotation rates at the median radii with the actually measured average rotation velocities in spherical shells near these radii. The collective rotation ('wave') is slower than the particle rotation both in the centre and towards the outside, but faster in the intermediate shell at $1.7\,r_H$.

Differential figure rotation in a triaxial model might be expected to result in different shells torquing one another. Such torques could, however, be substantially averaged out when resonances are important. It is interesting that the rotation rate in shell 3 (S3) is slightly more than one-half that in S1 and S2 and this may be an explanation for why the state of differential figure rotation survives for so long. Some non-systematic changes are visible in Fig. 1: the possible acceleration in S3 initially, or the later acceleration in S2 which may be related to the decelerations in S1 at $t = 4\,t_{cr}$ and $t = 6\,t_{cr}$. The model has been evolved for a further $4\,t_{cr}$ beyond the time-interval plotted. No gradual alignment of the major axes at different radii appears to develop, but the system becomes systematically rounder and after $t = 7\,t_{cr}$ the analysis method is frequently at or beyond its limits so that no further continuation of Fig. 1 is possible. The rate of evolution is faster in the plane ellipticity ($\Delta\epsilon_b \approx -0.19/10\,t_{cr}$) than in the perpendicular ellipticity ($\Delta\epsilon_c \approx -0.07/10\,t_{cr}$). This and the fact that we have found no evidence for two-body relaxation in a mass-segregation test suggest that the torques may cause a genuine secular evolution. The time-scale of this evolution is $\approx 10\,t_{cr}$.

Table 1. Figure rotation and particle rotation in model ME.

r/r_H	rotation rate ($^\circ/t_{cr}$)	v_r (fig)	v_r (meas)
0.22	82	0.75	1.7
0.63	78	2.0	2.4
1.7	47	3.3	2.1
7.0	1.5	0.43	0.9

4 A model with intrinsic principal axes twists

The second model (hereafter: model MD) resulted from the merging of a version of model ME with heavy core particles and one of the merger remnants of Paper I, on a bound, head-on orbit. Here, the initial orbital direction and the angular momentum vector of the final remnant **L** formed an angle of 110°. Rotation is small in this model ($\lambda = 0.08, v_{max}/\sigma_0 = 0.13$); nevertheless **L** seems to play some role in determining the shape of the remnant: the angle between **L** and the minor axis is 10–30°, depending on radius and time, so close to but significantly greater than zero.

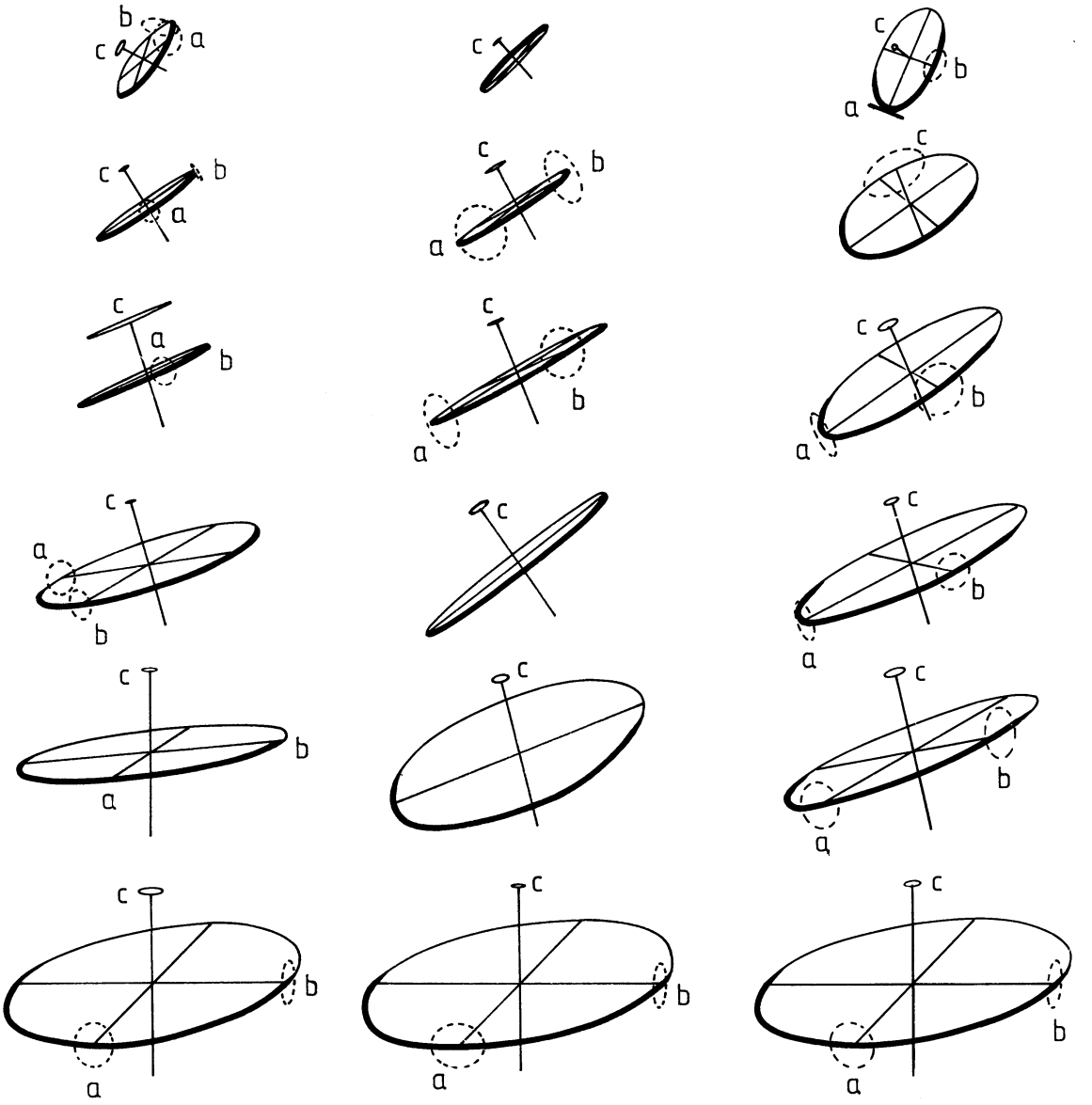

Figure 2. Perspective projection of the principal axes in model MD as a function of radius, for three snapshots at times $t = 3\,t_{cr}$ (a), $t = 9\,t_{cr}$ (b) and $t = 15\,t_{cr}$ (c) after equilibrium was reached. All directions are drawn relative to those of the outermost shell which very nearly remain unchanged during the simulation. The bold side of the ellipse representing the major plane comes out of the projection plane towards the reader. Its unprojected axial ratio is that determined by the procedure described in the text. The small circles correspond to the cones whose opening angle 2θ is twice the rms uncertainty of the direction of the corresponding axis. When no such error circles are shown, two axes are nearly equally long and their directions are very uncertain.

Model MD is also triaxial, with $\epsilon_c \approx 0.4$, $\epsilon_b \approx 0.2$. The data may indicate some non-systematic changes in the ellipticities but these are not very significant in view of the errors involved. This shape is again largely caused by velocity anisotropy. However, the directions of the major axes determined for all particles in six concentric spherical shells change radially in a complex way that is perhaps best described by imagining a coordinate system with one axis parallel to and moving along a curved path, with the other two rotating slowly about this axis at the same time. We have attempted to illustrate this behaviour by a perspective projection in Fig. 2. The large ellipse in each frame represents the major plane and has the measured axial ratio when unprojected. The small circles indicate the uncertainties in the directions of the respective axes. Their radii correspond to the rms deviations from the mean directions in the corresponding Monte Carlo simulation. These simulations resulted in a table of mean coordinate magnitude ratios **x** and rms direction errors for each radial shell as a function of two ellipticities. The set of values **x** fitting any given analysed shell best was then used to determine the other quantities. Fig. 2 suggests that (i) this model has significant intrinsic principal axis twists as a function of radius, (ii) these twists are basically long-lasting (until $15\,t_{cr}$ after equilibrium was reached), although some evolution in detail may be present. The magnitude of the twist angle between the minor axes of the innermost and outermost shells is up to one radian.

5 Conclusion

The results of the last two sections indicate that intrinsic twists of the principal axes of ellipsoidal stellar systems are permitted to last over astronomically significant time-intervals. Hence it is natural to suspect that some of the elliptical galaxies showing isophote twists and ellipticity variations with radius may be in similar states. It is not clear, however, whether such a configuration can be a strict equilibrium, or whether the system evolves slowly through a sequence of such states. Future work will have to assess the significance of secular evolution on time-scales similar to that found in the first model described above or longer for the dynamics of elliptical galaxies.

Acknowledgments

I thank Drs J. Binney and G. Efstathiou for helpful discussions. This work was funded partly by the Studienstiftung des Deutschen Volkes and partly by ESA.

References

Bertola, F. & Galetta, G., 1979. *Astr. Astrophys.*, **77**, 363.
Binney, J., 1978a. *Mon. Not. R. astr. Soc.*, **183**, 501.
Binney, J., 1978b. *Comments Ap.*, **8**, 27.
Carter, D., 1978. *Mon. Not. R. astr. Soc.*, **182**, 797.
di Tullio, G. A., 1979. *Astr. Astrophys. Suppl.*, **37**, 591.
Gerhard, O. E., 1981. *Mon. Not. R. astr. Soc.*, **197**, 179.
Gerhard, O. E., 1983. *Mon. Not. R. astr. Soc.*, **202**, 1159.
King, I. R., 1978. *Astrophys. J.*, **222**, 1.
Leach, R., 1981. *Astrophys. J.*, **248**, 485.
White, S. D. M.. 1978. *Mon. Not. R. astr. Soc.*, **184**, 185.
Williams, T. B. & Schwarzschild, M., 1979. *Astrophys. J.*, **227**, 56.